Direct observation of the Mottness and p-d orbital hybridization in epitaxial monolayer α-RuCl3

Zhongjie Wang (zhongjiewang18@fudan.edu.cn)
Fudan university, China https://orcid.org/0000-0002-9997-4248

Lu Liu
Fudan university, China

Haoran Zheng
Fudan university, China

Meng Zhao
Fudan university, China

Ke Yang
Fudan University

Chunzheng Wang
Fudan university, China

Fang Yang
Institute for Nanoelectronic Devices and Quantum Computing, Fudan University, Songhu Rd. 2005, 200438 Shanghai https://orcid.org/0000-0002-9152-1260

Hua Wu
Fudan University https://orcid.org/0000-0003-1280-202X

Chun-Lei Gao
Fudan University

Article

Keywords: α-RuCl3, chemical physics, nanoscience

Posted Date: July 12th, 2021

DOI: https://doi.org/10.21203/rs.3.rs-646319/v1

Abstract

α-$RuCl_3$, with abundant studies in its bulk phase, has shown the promising potential to approach the two-dimensional Kitaev honeycomb model and to realize the consequential quantum spin liquids. In this material, some ingredients spark off the hunting of quantum spin liquid states: the localized magnetic moments on each Ru^{3+} ion guaranteed by the Mottness, the Kitaev-type interaction originating from the superexchange path over the p-d bonds, and the nearly two-dimensional nature of the van der Waals coupled honeycomb layers. Here, we worked out the growth art of α-$RuCl_3$ monolayer on highly oriented pyrolytic graphite substrate for the first time, and then studied its electronic structure, particularly the delicate orbital occupations. Through scanning tunneling microscopy and spectroscopy study, the bonding configurations are justified by the features of pronounced t_{2g}-p_π and e_g-p_σ hybridization, and the Mott nature is unveiled by an ~ 0.6 eV full gap at the Fermi level located in the t_{2g}-p_π level. Our experimental results agree well with the density functional theory calculations of the monolayer system. In accordance with previous theoretical research, the epitaxial monolayer α-$RuCl_3$ system holds high tunability comparing to its bulk phase and provides a novel platform to explore the Kitaev physics.

Introduction

α-$RuCl_3$ is gifted of yielding quantum spin liquid (QSL) state, the prominent elusive phase of matter that exhibits high entanglement and topological order, through the intrinsic frustration embedded in the Kitaev-type bond-dependent interactions of magnetic moments in a honeycomb lattice[1–6]. Conforming to the Jackeli-Khaliullin mechanism, a strong Coulomb repulsion localizes the spin-orbit entangled J_{eff}=1/2 moments in Mott-insulating α-$RuCl_3$, and the Kiteav interaction emerges from the superexchange process through the Ru-Cl-Ru path over its t_{2g}-p_π bonds (namely the t_{2g}-p_z bonds in their proposal[1]). Therefore, it has attracted enormous studies on α-$RuCl_3$ which show evidences of Kitaev-type magnetic interactions and itinerant Majorana fermions in the bulk phase[7–14].

Comparing to the bulk, monolayer α-$RuCl_3$ is closer to the two-dimensional Kitaev model since the stacking faults in bulk may cause additional magnetic transitions at 8-14K[15,16]. In addition, the electronic and magnetic properties of monolayer are more tunable by the application of strain, doping, and interfacial effect which were recently predicted to be promising routes in searching for novel states of matter[17–20]. However, it has been difficult to synthesize high-quality, high-coverage, and chemically pure monolayer α-$RuCl_3$ which enables access to its intrinsic properties, and the study of monolayer α-$RuCl_3$ remains scarce and challenging.

In this work, we successfully synthesized high-quality monolayer α-$RuCl_3$ on highly oriented pyrolytic graphite (HOPG) substrate by molecular beam epitaxy (MBE). Through low-temperature scanning tunneling microscopy (STM) and spectroscopy (STS) studies, we found an in-plane lattice expansion in the α-$RuCl_3$ monolayer compared to bulk and the persistence of the Mott nature as evidenced by an ~ 0.6

eV full Mott gap. Noting that the previous STM work on the α-$RuCl_3$ thin film (≈ 15–30 layers) shows an ~ 0.25eV gap[21], the gap size of the monolayer is significantly magnified, which could result from the enhancement of the Coulomb correlation due to the reduced electronic screening in a two-dimensional system[22–24]. The observed electronic states agree with the distinct features of t_{2g}-p_π and e_g-p_σ bonds. Both the energy spectroscopy and the real-space images are in good agreement with density functional theory (DFT) calculations. The Mott gap in the t_{2g} manifold is justified by a comprehensive study of experiment and theory. Our attempts of the structural modification via interfacial effect on the monolayer scale are a rehearsal of tuning the relevant electronic/magnetic properties and exploring the Kitaev physics in α-$RuCl_3$[17,25–27].

Results

Synthesis and topography of $RuCl_3$]

Two structural phases of $RuCl_3$ thin films were found in the growth process. First, β-$RuCl_3$ chains and disordered α-$RuCl_3$ fragments are self-assembled on the surface. Highly ordered α-$RuCl_3$ monolayer appears and proliferates gradually in the annealing process. Figure 1(a)[(b)] shows the crystal structure of monolayer α-$RuCl_3$ (β-$RuCl_3$) where the edge (face)-sharing $RuCl_6$-octahedra constitute the honeycomb lattice (zigzag chains) of α-form (β-form). In bulk, the β-phase is metastable and can be converted to α-phase at 450–600 ^oC [30] and Fig. 1(c) shows the RHEED patterns of the sample after preliminary growth, further deposition, and annealing from the top down. The preliminary growth of submonolayer $RuCl_3$ gives the RHEED pattern [Top of Fig. 1(c)] of only β-phase and the corresponding STM image is given in Fig. 1 (d). Further deposition leads to the coexistence of α- and β-phase as shown in the RHEED pattern [middle of Fig. 1(c)]. Nanoscale STM topography [Fig. 1(e)] reveals compact domains of poorly ordered α-area and highly crystalized β-area. The image Fig. 1(f) gives the detailed structure of β-$RuCl_3$ which shows neck-and-neck zigzag chains. The lattice constants of a = 5.5 Å, b = 6.1 Å are straightforward indications of β-$RuCl_3$[31]. Post annealing of fully covered monolayer film does not cause a significant change of lattice constant [bottom of Fig. 1(c)]. However, a structural phase transition is inferred by the STM topographic image [Fig. 1(h)], where a reduction of coverage [Fig. 1(g)] and a proliferation of α-$RuCl_3$ monolayer with β-$RuCl_3$ dressed in pieces can be seen. A blurred triangular lattice resolved at high tunneling resistance [Fig. 1(i)] stands for α-$RuCl_3$ (See Fig. 3 for details) with a lattice constant of 6.19 Å, which can be well distinguished from the rectangular lattice of β-$RuCl_3$. Comparing to 5.99 Å in the bulk[31], the in-plane lattice constant of the α-$RuCl_3$ layer is expanded by 3%, which fits the expectation for this heterostructure[17].

Electronic properties and orbital textures of d-p bonds

Figure 2(a) shows the typical dI/dV experimental spectrum of α-$RuCl_3$ monolayer (black solid line) and the calculated total DOS where majority and minority spins are represented by green and orange dashed

lines respectively.The total DOS was given by the LSDA + SOC + U calculations, where the lattice constant a = b = 6.19 Å and a vacuum spacing of 15 Å were employed. The DFT calculations come out with a Mott phase and an energy splitting of t_{2g} orbitals, which well explain the STS result. The Mott nature is supported by an ~ 0.6 eV full gap around Fermi level in the experimental curve. The ~ 1.0 eV peak-to-peak Mott gap is consistently given by both the experiment and calculation as marked in Fig. 2(a). In Fig. 2(b), the calculated partial density of states (PDOS) graph exhibits an ~ 2.0 eV splitting of t_{2g} and e_g orbitals due to the octahedral crystal field. The Cl-3p orbital occupies the valence band below $\approx$ -2.0 eV, while the Ru-4d orbital resides between $\approx$ -2.0 eV and $\approx$ 3.0 eV. Meanwhile, the orbital hybridization induces the mixture of p and d components in the whole energy scale. We projected the p orbitals onto the degeneracy-lifting basis of p_π and p_σ orbitals and found that, specifically, the hybridization undergoes in the manner of t_{2g}-p_π and e_g-p_σ bonding in Fig. 2(b). In the energy range of t_{2g} orbitals, the PDOS of the p_π component is much larger than the p_σ one due to the dominant pdπ bonding. In the energy range of e_g orbitals, instead, the p_σ component is much larger due to the pdσ bonding.

As expected, we observed distinct STM patterns in the energy ranges of different orbitals. Figure 3(a-f) are the typical constant-current STM images at indicated bias voltages. In the t_{2g} and p_π dominating energy range (-3.0 to 1.5 eV), three protrusions are resolved in each surface unit cell forming a “Kagome-like” lattice. However, in the energy range of e_g orbital, only one protrusion is observed appearing as a cluster of three, forming a triangular lattice of the trimers. Similar phenomena were observed in the STM images of CrI_3 thin film[33]. Figure 3(g, h) show the simulated constant-current STM images, i.e. the isosurface of DOS integrated from Fermi level to the bias energy, based on Tersoff-Hamann model[34]. Figure 3(g) is the typical simulated image at 0.9V while all the images of the t_{2g} range show the same “Kagome-like” pattern. It is found that the images can be well explained by the two types of the Cl-3p states, specifically the p_π type for Fig. 3(g) and the p_σ type for Fig. 3(h). In detail, the lobes of p_π are perpendicular to the corresponding Ru_2Cl_2 plane which is formed by two Ru ions and two bridging Cl ions [the case of experimental images Fig. 3(a-e) and the simulated image Fig. 3(g)], while the lobes of p_σ lie in the Ru_2Cl_2 plane [the case of the experimental image Fig. 3(f) and the simulated image Fig. 3(h)]. The t_{2g} (e_g) orbital primarily hybridizes with the p_π (p_σ) orbital based on the large orbital overlap and thus forms the pdπ (pdσ) bond. The STM images are dominated by the upper lobes of the topmost Cl- p_π and Cl- p_σ states which reside on the opposite sides of the Cl ion and evolve into the vacuum. The distinct orientations of the Cl-p states of two types produce the shift (orange and green arrows) of image intensity with respect to the Cl atom sites (blue balls) as marked in Fig. 3(g, h). Thus, Cl- p_π and Cl- p_σ orbitals directly link to the t_{2g} and e_g orbitals surrounding the Ru atoms, respectively. The same t_{2g}- p_π textures across the fermi level clearly illustrates the monolayer system remains in Mott phase.

Conclusions

In conclusion, the strained α-$RuCl_3$ monolayer interfacing graphite was fabricated by the method of MBE. The p-d hybridization was directly visualized and understood and the Mott insulating behavior of α-$RuCl_3$

monolayer was validated by the accordant STM measurements and DFT calculations. The monolayer system enables the local tunneling probes to join the search of topological quantum magnets as a powerful weapon targeting the atomic-scale structure, electronic properties, and correlations, microscopic magnetic order as well as the excitation of unusual quasiparticle[35–37]. The strained α-$RuCl_3$ would definitely make the spin-orbital structure, as well as inherent magnetic interactions, differ from the bulk system. Besides the stretched lattice (and the widened Ru-Cl-Ru bond angle) which may be advantageous for the advancement toward Kitaev limit [17,26,27,38,39], the magnetic anisotropy of the system could have a favorable out-of-plane easy axis. Thus, it's intriguing and worth more studies that what the exact magnetic ground order is.

Methods

The α-$RuCl_3$ monolayer was grown on cleaved HOPG by MBE at a base pressure of ~ 1×10^{-9} mbar. The commercial anhydrous $RuCl_3$ powder was evaporated at 324 ^{o}C and the substrate was kept at 180 ^{o}C during film growth. After the growth, the $RuCl_3$ sample was annealed up to 317 ^{o}C in half an hour. The process of growth was monitored by reflective high-energy electron diffraction (RHEED). The subsequent in situ STM and STS measurements were done at 5 K with tungsten tips. DFT calculations were performed by the full-potential augmented plane wave plus local orbital code (Wien2k)[28]. The muffin-tin sphere radii of Ru and Cl atoms were chosen to be 2.2 and 2.1 Bohr, respectively. The plane-wave cut-off energy for interstitial wave functions was set to be 14 Ry. The integration over the Brillouin zone was carried out on a 14×14×1 k-mesh. To account for the electron correlation, the local spin density approximation plus Hubbard U (LSDA + U) method[29] was employed and typical values of Hubbard U = 3.0 eV and Hund exchange J_H=0.5 eV were used for Ru 4d states. The spin-orbit coupling (SOC) was included for Ru 4d and Cl 3p orbitals via the second-variational method with scalar relativistic wave functions.

Declarations

ACKNOWLEDGMENTS

C. G. acknowledges funding from the National Key Research and Development Program of China (Grant No. 2019YFA0308404, 2016YFA0300904), National Natural Science Foundation of China (Grant No. 11427902 and 11674063), Science and Technology Commission of Shanghai Municipality (Grant No. 20JC1415900) and Shanghai Municipal Science and Technology Major Project (Grant No.2019SHZDZX01). H. W. acknowledges support from the NSF of China (Grant No. 11674064) and the National Key Research and Development Program of China (Grant No. 2016YFA0300700). F. Y. is sponsored by Shanghai Pujiang Program No. 19PJ1401000 and National Natural Science Foundation of China (Grant No. 12004076).

Z. W. and L. L. contribute equally to this work.

References

1. G. Jackeli and G. Khaliullin, *Mott Insulators in the Strong Spin-Orbit Coupling Limit: From Heisenberg to a Quantum Compass and Kitaev Models*, Phys. Rev. Lett. **102**, 017205 (2009).
2. J. Chaloupka, G. Jackeli, and G. Khaliullin, *Kitaev-Heisenberg Model on a Honeycomb Lattice: Possible Exotic Phases in Iridium Oxides A_2IrO_3*, Phys. Rev. Lett. **105**, 027204 (2010).
3. K. W. Plumb, J. P. Clancy, L. J. Sandilands, V. V. Shankar, Y. F. Hu, K. S. Burch, H.-Y. Kee, and Y.-J. Kim, *$\alpha - RuCl_3$: A spin-orbit assisted Mott insulator on a honeycomb lattice*, Phys. Rev. B **90**, 041112(R) (2014).
4. H.-S. Kim, V. V. Shankar, A. Catuneanu, and H.-Y. Kee, *Kitaev magnetism in honeycomb $RuCl_3$ with intermediate spin-orbit coupling*, Phys. Rev. B **91**, 241110(R) (2015).
5. A. Koitzsch, C. Habenicht, E. Müller, M. Knupfer, B. Büchner, H. C. Kandpal, J. van den Brink, D. Nowak, A. Isaeva, and Th. Doert, *Jeff Description of the Honeycomb Mott Insulator $\alpha - RuCl_3$*, Phys. Rev. Lett. **117**, 126403 (2016).
6. L. Balents, *Spin liquids in frustrated magnets*, Nature **464**, 199 (2010).
7. L. J. Sandilands, Y. Tian, K. W. Plumb, Y.-J. Kim, and K. S. Burch, *Scattering Continuum and Possible Fractionalized Excitations in $\alpha - RuCl_3$*, Phys. Rev. Lett. **114**, 147201 (2015).
8. A. Little, Liang Wu, P. Lampen-Kelley, A. Banerjee, S. Patankar, D. Rees, C. A. Bridges, J.-Q. Yan, D. Mandrus, S. E. Nagler, and J. Orenstein, *Antiferromagnetic Resonance and Terahertz Continuum in $\alpha - RuCl_3$*, Phys. Rev. Lett. **119**, 227201 (2017).
9. Z. Wang, S. Reschke, D. Huvonen, S.-H. Do, K.-Y. Choi, M. Gensch, U. Nagel, T. Room, and A. Loidl, *Magnetic Excitations and Continuum of a Possibly Field-Induced Quantum Spin Liquid in $\alpha - RuCl_3$*, Phys. Rev. Lett. **119**, 227202 (2017).
10. A. Banerjee, J. Yan, J. Knolle, C. A. Bridges, M. B. Stone, M. D. Lumsden, D. G. Mandrus, D. A. Tennant, R. Moessner, and S. E. Nagler, *Neutron scattering in the proximate quantum spin liquid α-$RuCl_3$*, Science **356**, 1055 (2017).
11. K. Ran, J. Wang, W. Wang, Z.-Y. Dong, X. Ren, S. Bao, S. Li, Z. Ma, Y. Gan, Y. Zhang *et al.*, *Spin-Wave Excitations Evidencing the Kitaev Interaction in Single Crystalline $\alpha - RuCl_3$*, Phys. Rev. Lett. **118**, 107203 (2017).
12. S.-H. Do, S.-Y. Park, J. Yoshitake, J. Nasu, Y. Motome, Y. S. Kwon, D. T. Adroja, D. J. Voneshen, K. Kim, T.-H. Jang *et al.*, *Majorana fermions in the Kitaev quantum spin system α-$RuCl_3$*, Nat. Phys. **13**, 1079 (2017).
13. Y. Kasahara, K. Sugii, T. Ohnishi, M. Shimozawa, M. Yamashita, N. Kurita, H. Tanaka, J. Nasu, Y. Motome, T. Shibauchi *et al.*, *Unusual Thermal Hall Effect in a Kitaev Spin Liquid Candidate $\alpha - RuCl_3$*, Phys. Rev. Lett. **120**, 217205 (2018).
14. Y. Kasahara, T. Ohnishi, Y. Mizukami, O. Tanaka, S. Ma, K. Sugii, N. Kurita, H. Tanaka, J. Nasu, Y. Motome *et al.*, *Majorana quantization and half-integer thermal quantum Hall effect in a Kitaev spin*

liquid, Nature **559**, 227 (2018).

15. R. D. Johnson, S. C. Williams, A. A. Haghighirad J. Singleton, V. Zapf, P. Manuel, I. I. Mazin, Y. Li, H. O. Jeschke, R. Valenti and R. Coldea, *Monoclinic crystal structure ofα − RuCl3and the zigzag antiferromagnetic ground state*, Phys Rev B **92**, 235119 (2015).
16. H. B. Cao, A. Banerjee, J.-Q. Yan, C. A. Bridges, M. D. Lumsden, D. G. Mandrus, D. A. Tennant, B. C. Chakoumakos, and S. E. Nagler, *Low-temperature crystal and magnetic structure of α-$RuCl_3$*, Phys Rev B **93**, 134423 (2016).
17. S. Biswas, Y. Li, S. M. Winter, J. Knolle, and R. Valentí, *Electronic Properties of α − $RuCl_3$ in Proximity to Graphene*, Phys. Rev. Lett. **123**, 237201 (2019).
18. E. Gerber, Y. Yao, T. A. Arias, and E.-A. Kim, *Ab Initio Mismatched Interface Theory of Graphene on α − $RuCl_3$: Doping and Magnetism*, Phys. Rev. Lett. **124**, 106804 (2020).
19. E. Vatansever, S. Sarikurt, F. Ersan, Y. Kadioglu, O. Üzengi Aktürk, Y. Yüksel, C. Ataca, E. Aktürk, and Ü. Akıncı, *Strain effects on electronic and magnetic properties of the monolayer α-$RuCl_3$: A first-principles and Monte Carlo study*, J. Appl. Phys. **125**, 083903 (2019).
20. F. Iyikanat, M. Yagmurcukardes, R. T. Senger, and H. Sahin, *Tuning electronic and magnetic properties of monolayer α-$RuCl_3$ by in-plane strain*, J. Mater. Chem. C. **6**, 2019 (2018).
21. M. Ziatdinov, A. Banerjee, A. Maksov, T. Berlijn, W. Zhou, H.B. Cao, J.-Q. Yan, C.A. Bridges, D.G. Mandrus, S.E. Nagler, A.P. Baddorf & S.V. Kalinin, *Atomic-scale observation of structural and electronic orders in the layered compound a-$RuCl_3$*, Nat Commun **7**, 13774 (2016).
22. Yi Chen, Wei Ruan, Meng Wu, Shujie Tang, Hyejin Ryu, Hsin-Zon Tsai,
23. Ryan Lee, Salman Kahn, Franklin Liou, Caihong Jia, Oliver R. Albertini, Hongyu Xiong†, Tao Jia, Zhi Liu†, Jonathan A. Sobota, Amy Y. Liu, Joel E. Moore, Zhi-Xun Shen†, Steven G. Louie†, Sung-Kwan Mo and Michael F. Crommie†, *Strong correlations and orbital texture in*
24. *single-layer 1T-$TaSe_2$*, Nature Physics **16**, 218 (2020).
25. Qiu, D. Y., da Jornada, F. H. & Louie, S. G, *Screening and many-body effects in two-dimensional crystals: monolayer MoS_2*. Phys. Rev. B **93**, 235435 (2016).
26. Miguel M. Ugeda, Aaron J. Bradley, Su-Fei Shi, Felipe H. da Jornada, Yi Zhang, Diana Y. Qiu, Wei Ruan, Sung-Kwan Mo, Zahid Hussain, Zhi-Xun Shen, Feng Wang, Steven G. Louie and Michael F. Crommie *Giant bandgap renormalization and excitonic efects in a monolayer transition metal dichalcogenide semiconductor*. Nat. Mater. **13**, 1091–1095 (2014).
27. S. M. Winter, A. A. Tsirlin, M. Daghofer, J. van den Brink, Y. Singh, P. Gegenwart, and R. Valenti, *Models and materials for generalized Kitaev magnetism*, J. Phys. Condens. Matter **29**, 493002 (2017).
28. H.-S. Kim and H.-Y. Kee, *Crystal structure and magnetism in α − $RuCl_3$: An ab initio study*, Phys. Rev. B **93**, 155143 (2016).
29. R. Yadav, N. A. Bogdanov, V. M. Katukuri, S. Nishimoto, J. van den Brink, and L. Hozoi, *Kitaev exchange and field-induced quantum spin-liquid states in honeycomb α-$RuCl_3$*, Sci. Rep. **6**, 37925 (2016).

30. P. Blaha, K. Schwarz, F. Tran, R. Laskowski, G. K. H. Madsen, and L. D. Marks, *WIEN2k: An APW + lo program for calculating the properties of solids*, J. Chem. Phys. **152**, 074101 (2020).
31. V. I. Anisimov, I. V. Solovyev, M. A. Korotin, M. T. Czyzyk, and G. A. Sawatzky, *Density-functional theory and NiO photoemission spectra*, Phys. Rev. B **48**, 16929 (1993).
32. J. M. Fletcher, W. E. Gardner, E. W. Hooper, K. R. Hyde, F. H. Moore, and J. L. Woodhead, *Anhydrous Ruthenium Chlorides*, Nature **199**, 1089 (1963).
33. H. Hillebrecht, T. Ludwig, and G. Thiele, *About Trihalides with TiI_3 Chain Structure: Proof of Pair Forming of Cations in β-$RuCl_3$ and $RuBr_3$ by Temperature Dependent Single Crystal X-ray Analyses*, Z. Anorg. Allg. Chem. **630**, 2199 (2004).
34. S.-Y. Park, S.-H. Do, K.-Y. Choi, D. Jang, T.-H. Jang, J. Schefer, C.-M. Wu, J. S. Gardner, J. M. S. Park, J.-H. Park., *Emergence of the Isotropic Kitaev Honeycomb Lattice with Two-dimensional Ising Universality in α-$RuCl_3$*, arXiv:1609.05690 (2016).
35. P. Li, C. Wang, J. Zhang, S. Chen, D. Guo, W. Ji, and D. Zhong, *Single-layer CrI_3 grown by molecular beam epitaxy*, Sci. Bull. **65**, 1064 (2020).
36. J. Tersoff and D. R. Hamann, *Theory and Application for the Scanning Tunneling Microscope*, Phys. Rev. Lett. **50**, 1998 (1983).
37. E. J. König, M. T. Randeria, and B. Jäck, *Tunneling spectroscopy of quantum spin liquids*, arXiv:2008.02278 (2020).
38. M. Udagawa, S. Takayoshi, and T. Oka, *STM as a single Majorana detector of Kitaev's chiral spin liquid*, arXiv:2008.07399 (2020).
39. D. F. Mross and T. Senthil, *Charge Friedel oscillations in a Mott insulator*, Phys. Rev. B **84**, 041102(R) (2011)
40. S. M. Winter, Y. Li, H. O. Jeschke, and R. Valentí, *Challenges in design of Kitaev materials: Magnetic interactions from competing energy scales*, Phys. Rev. B **93**, 214431 (2016).
41. R. Yadav, S. Rachel, L. Hozoi, J. van den Brink, and G. Jackeli, *Strain- and pressure-tuned magnetic interactions in honeycomb Kitaev materials*, Phys Rev B **98**, 121107(R) (2018).

Figures

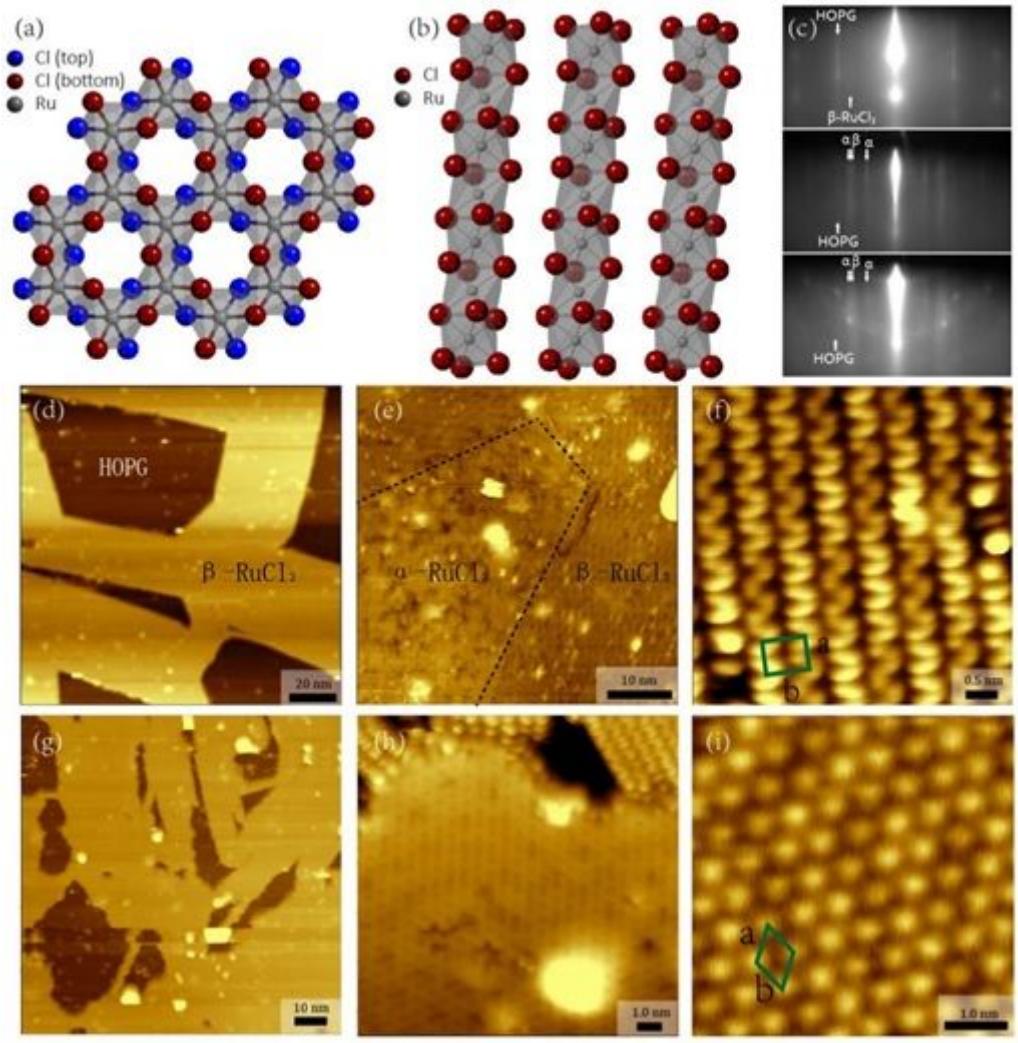

Figure 1

Structure and STM topography of RuCl3. (a,b) Atomic structures of α-RuCl3 and β-RuCl3. (c) RHEED patterns of β-RuCl3 grown on HOPG substrate after preliminary deposition (top) and β-RuCl3 as well as amorphous α-RuCl3 grown during further deposition (middle) and sample after annealing at 317 oC (bottom). The diffraction stripes of HOPG, β-RuCl3, and α-RuCl3 are indicated. (d) Large scale STM image of β-RuCl3 chains after preliminary growth (U=1.9 V, I=100 pA). (e) STM image shows the coexistence of β-RuCl3 chains and amorphous α-RuCl3 after further deposition (U=1.6 V, I=100 pA). (f) High-resolution image of β-RuCl3 (U=1.4 V, I=100 pA). (g-i) STM images after post-annealing. (g,h) Large scale and small scale images show the coexistence of both forms of RuCl3 (g: U=2.3 V, I=100 pA, h: U=1.5 V, I=300 pA). (i) STM image of α-RuCl3 (U=2.8 V, I=100 pA) shows a triangular lattice with a 6.19 Å lattice constant.

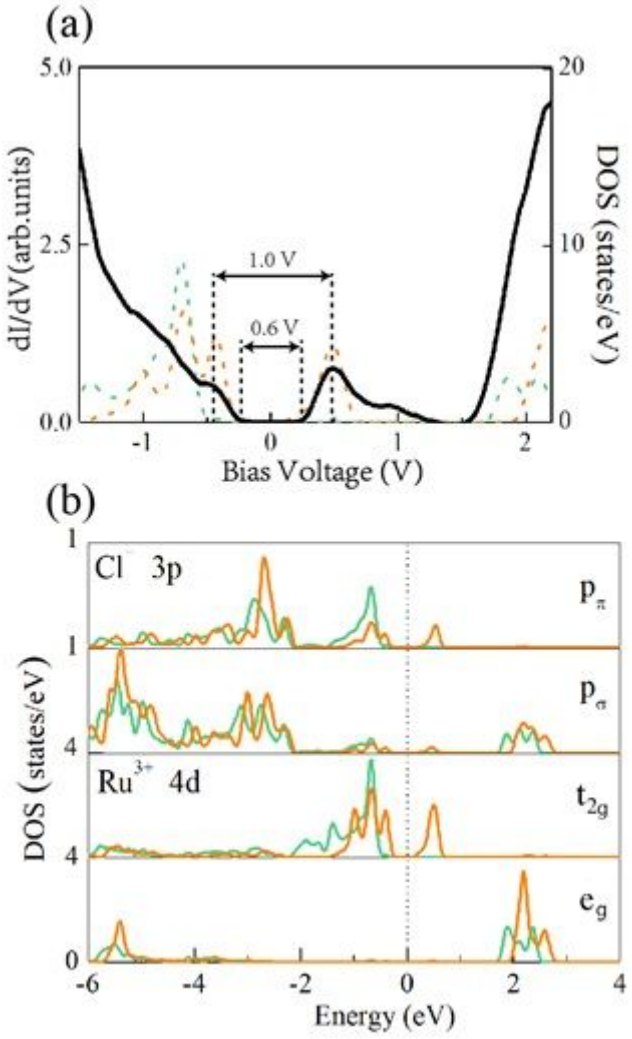

Figure 2

Spectrum and DFT results. (a) STS of α-RuCl3 monolayer (solid black line, U=2.2 V, I=5.8 nA, bias modulation amplitude ΔU=20 mV at frequency f=983 Hz) and calculated total DOS for the ground state of the α-RuCl3 monolayer by LSDA+SOC+U, the dashed green (orange) curve describes the majority (minority) spins. The size of the full gap and the peak-to-peak gap is indicated. (b) The orbital PDOS of the α-RuCl3 monolayer. The green (orange) curves describe the majority (minority) spins and the Fermi level is set to the middle of the gap.

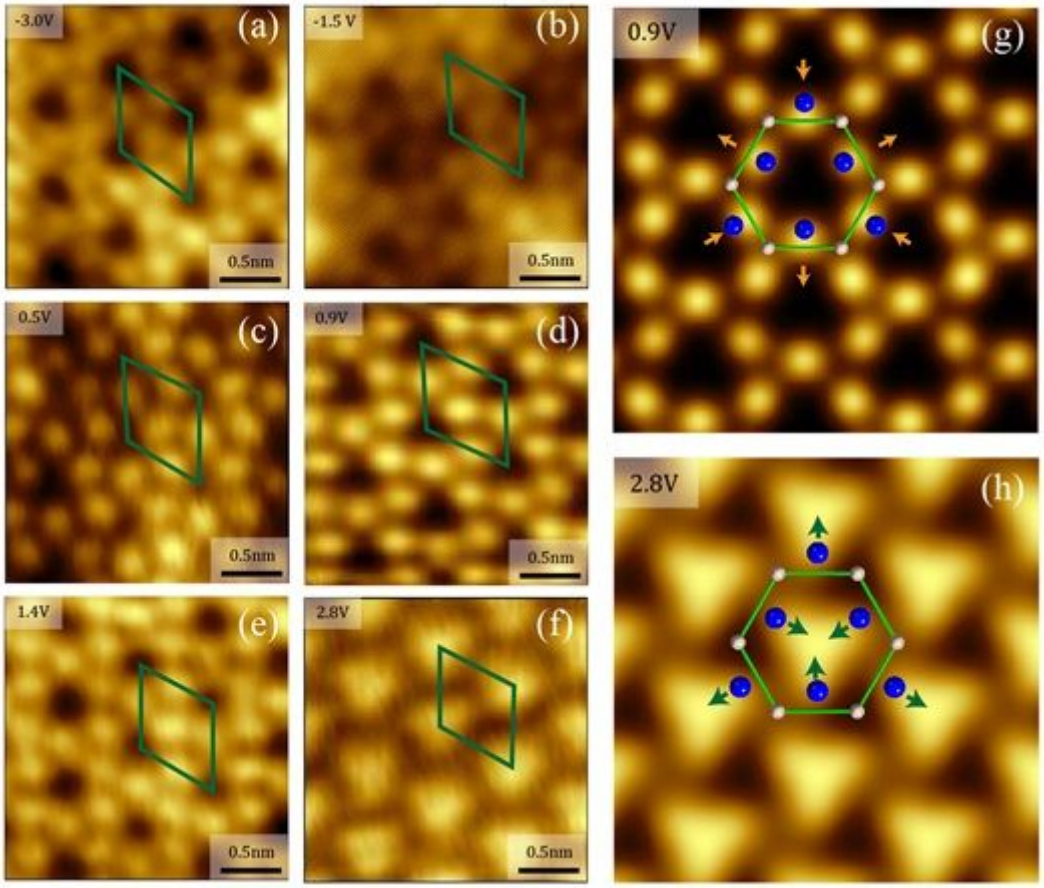

Figure 3

energy-resolved orbital textures. (a-f) Bias-dependent STM images in the constant-current mode. (a: U=-3.0 V, I=-15 nA. b: U=-1.5 V, I=-10 nA. c: U=0.5 V, I=0.5 nA. d: U=0.9 V, I=0.6 nA. e: U=1.4 V, I=0.6 nA. f: U=2.8 V, I=100 pA). (g, h): The representative constant-current-image simulations at 0.9 V with the distorted “Kagome” lattice and 2.8 V with the triangularly arranged trimers, respectively. The Ru-hexagon (gray balls) and topmost Cl ions (blue balls) are put at the right positions in the lattice. The orange and green arrows represent the displacement from Cl sites to the bright protrusions.